IEEE Open Journal of
Antennas and Propagation

Received 16 October 2020; revised 18 November 2020; accepted 22 November 2020. Date of publication 14 December 2020;
date of current version 25 January 2021.

Digital Object Identifier 10.1109/OJAP.2020.3044471

Wideband Dipole Array With Balanced Wideband Impedance Transformer (BWIT)

ALEXANDER D. JOHNSON (Member, IEEE), JINGNI ZHONG (Member, IEEE), MATILDA LIVADARU (Member, IEEE), SATHEESH BOJJA VENKATAKRISHNAN (Member, IEEE), ELIAS A. ALWAN (Member, IEEE), AND JOHN L. VOLAKIS (Fellow, IEEE)

Department of Electrical and Computer Engineering, College of Engineering and Computing, Florida International University, Miami, FL 33174, USA

CORRESPONDING AUTHOR: S. B. VENKATAKRISHNAN (e-mail: sbojjave@fiu.edu)

ABSTRACT Within the context of modern digital phased array (DPA) radios, differential Radio Frequency (RF) front-ends provide much greater immunity to noise and distortion by suppressing second order harmonics. Recent advancements in differential RF front-ends offer high dynamic range, high linearity, and low noise in the transceiver chain. However, a major roadblock to fully differential systems is the presence of common-mode resonances. In this article, we present a novel wideband differential feed for dipole arrays that overcomes this bottleneck. Our dipole array is developed for the L-S band (*viz.* 1.05 GHz to 3.2 GHz) with emphasis on dual-linear polarization and resonance-free scanning to low angles. The novelty of this article is the Balanced Wideband Impedance Transformer (BWIT) feed that mitigates common-mode currents across the entire band while scanning to low angles. Array simulations are verified with measurements of an 8×8 prototype in a volume of 384mm×384mm×57mm. The array achieves resonance-free scanning across a 3:1 impedance bandwidth with VSWR < 3 for the cases of $\theta = 0°$ (Broadside), 45° (D-plane), 60° (E-plane) and across a 2.37:1 impedance bandwidth with VSWR < 3 for the case of 45° (H-plane). Measured gain achieves near-theoretical values across the operating band.

INDEX TERMS Antenna arrays, differential geometry, phased arrays, ultra-wideband antennas.

I. INTRODUCTION

WIDEBAND antennas and arrays are essential for high data rate communications and software defined radios (SDRs). Wideband systems also enable increased spectral efficiency, increased data rates, Multiple-Input-Multiple-Output (MIMO) and secure spread spectrum communications. For many applications, these arrays would require a wide angle scanning range for comprehensive spatial coverage. Notably, wideband arrays can replace several narrowband antennas to reduce power, cost, and space requirements. In this article, we are aiming at multi-functional array, specifically for base-station communications with applications to 4G LTE (long term evolution), the new AWS-3 (Advanced Wireless Service) and "mid-band 5G" bands.

As mobile communication systems continue to develop, it is apparent that wideband, high gain, low-cost antennas are needed to keep pace with data rates, especially in the band from 1-3 GHz [1]. More specifically, the second generation (2G) systems operated in the frequency bands 1710-1880 MHz (GSMA 1800) and 1850-1990 MHz (GSMA 1900), while the third generation (3G) systems like CDMA 2000 and WCDMA use the frequency band 1920-2170 MHz. The LTE 4G systems, such as LTE2300 and LTE2500 use designated frequency bands 2300-2400 MHz and 2500-2690 MHz, and the AWS bands 1700-2100 MHz with the 3G technology. Also, the GPS L1, L2 an L5 bands (1575, 1227, 1176 MHz, respectively.) are integral to today's communication systems. Furthermore, the "mid-band 5G" technology systems uses a similar frequency range, from 2300 to 2600 MHz. Thus, an UWB array with wide-angle scanning in the 1-3 GHz band is beneficial for 2G/3G/4G/5G base stations, as it reduces hardware complexity.

TABLE 1. Dimensions (units : mm) of array in Fig. 1(c).

A	B	C	D	E	F	G	H	I
22.8	25.2	11.8	2.1	2.6	33	0.58	10.8	48
J	**K**	**L**	**M**	**N**	**O**	**P**	**Q**	**R**
5.6	11	0.91	22.9	7.6	11.33	0.91	0.25	0.91

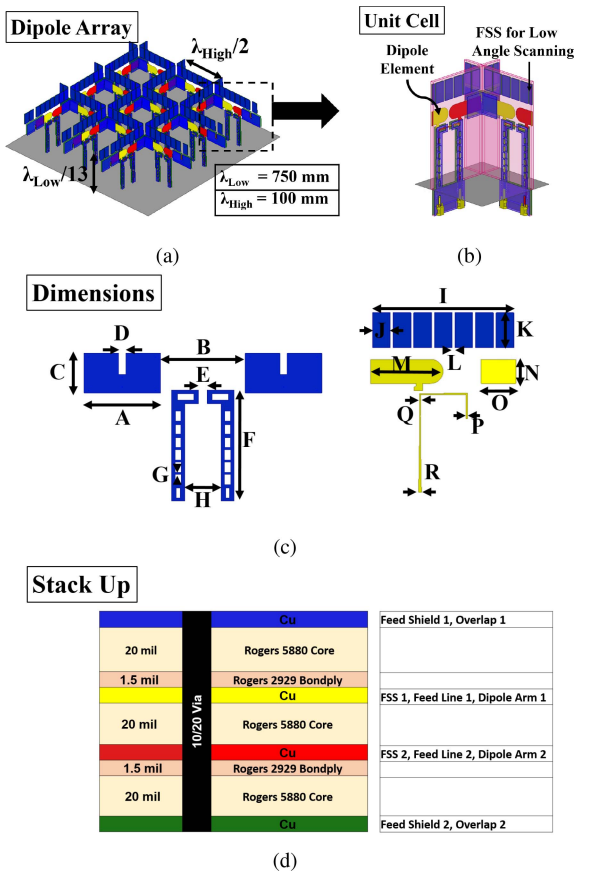

FIGURE 1. Pictorial representation of (a) the dual-polarized dipole array and (b) its infinite array unit cell. The (c) dimensions of the design and (d) a printed circuit board stack-up (color coded) are also given to show the layer details.

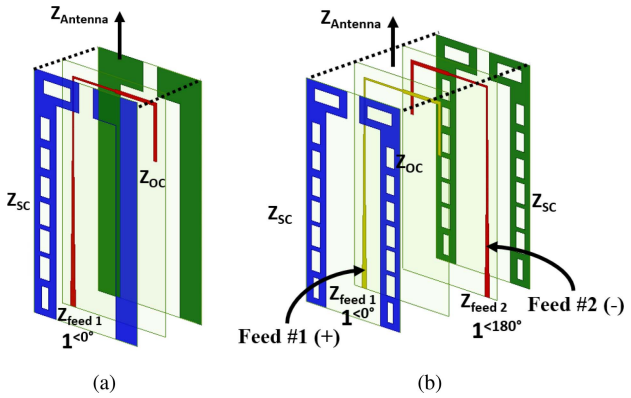

FIGURE 2. Pictorial representation of a (a) Marchand Balun and (b) BWIT feeds.

Concurrent to the aforementioned applications, there is a movement in RF hardware towards differential components [2]. Differential configurations enable high dynamic range, high linearity, and inherently lower distortions in response to noise and interference from power supplies. Distortions due to even order harmonics from nonlinear devices can also be suppressed by differential lines [3]. Further, differentially fed antennas (e.g., dipoles) are inherently compatible with differential amplifiers, thereby removing extraneous baluns across the RF chain and antenna feeds. The removal of these unnecessary balun stages, especially in the case of ultra-wideband (UWB) balun, significantly reduces associated losses and phase/amplitude mismatches.

Recently, many reduced size, weight, area, power and cost (SWAP-C) coupled dipole arrays have been developed for UWB and multi-functional operation to meet the aforementioned needs. Thus far, these have been implemented with a variety of accompanying feed designs [4]–[13]. Of course, a dipole array over a ground plane requires a balanced excitation at the dipole terminal that extends a distance H above the ground plane (where $\lambda/4 < H < \lambda/2$ to respect image theory). Notably, traditional differential feeds have inherent UWB performance at broadside, however, they exhibit common-modes when used in a phased array that scans to low angles [14], [15]. For instance, the UWB differential feeds in [16]–[19] exhibited common-mode resonances when scanning in the E-plane nearing angles of 45°. As is known, these common-modes arise for particular scan angles and frequencies in the differential feed lines due to destructive mutual coupling between elements in presence of a third conductor (i.e., ground plane). If not addressed properly, these common-modes radiate in a manner that significantly reduces the efficiency and usable bandwidth of balanced array structures (i.e., PEC backed dipoles) [14], [15]. Hence, a major challenge in the design of fully differential radios is the vertically oriented balanced feed that does not resonate when scanning across large bandwidths.

In the past, the most prevalent way to suppress scan-dependent common-modes was to employ a balanced-to-unbalanced feed (*viz* balun), thereby avoiding differential feeding altogether [5], [7]–[12], [14]. A typical wideband balun was the folded Marchand balun [5], [20], which has been adapted to higher frequencies [10], [21] and in novel fabrication methods [12]. However, as discussed above, this approach introduces the need for more baluns later in the predominantly differential RF chain. Other methods have been explored to mitigate such modes without a balun feed. For example, by employing conductive walls at the edges of the dipole arms for disruption of the coupled fields [16], [17], [22], yet this approach introduces design complexities in fabricating a non-planar ground plane. Also, resistive terminations have been used to attenuate the common-modes at the cost of efficiency [18], [19].

In this article, the novel dipole array in Fig. 1 is presented. This differentially fed array achieves continuous wide-angle scans across its wideband operation. To realize resonance-free scans, a new feed structure, referred to as the Balanced Wideband Impedance Transformer (BWIT), is presented

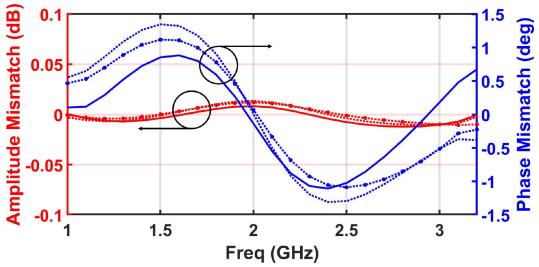

FIGURE 3. Amplitude variation and phase imbalance of BWIT feed for broadside (solid) 45° (dashed), and 60° (circle-dashed) scanning cases.

(see Fig. 2). Learning from the Marchand Balun's [5] common-mode immunity, this differential design employs a pair of reactive transmission line components to mitigate common-modes across a continuous 3:1 impedance bandwidth (VSWR $<$ 3) while scanning. In reference to the aforementioned common-mode mitigation techniques, the dipole array with BWIT successfully delivers a resonant-free scanning through a simple low-cost PCB printed feed, with no added fabrication steps or intentional losses. Simulations are verified with measurements of a fabricated 8 $\times$ 8 dual-polarized prototype. This article is organized as follows. Section II presents the design of the dual-polarized array with the novel differential BWIT feed, operating across 1.05 GHz to 3.2 GHz. Fabrication and measurement details are presented in Section III. Section IV gives comparisons of the presented array to other recent dipole arrays.

II. DIFFERENTIALLY FED DIPOLE ARRAY DESIGN

A. DIFFERENTIAL FEEDING NETWORK

As previously noted, several past dipole arrays employed an integrated Marchand balun [5], [20] with the characteristics of that in Fig. 2(a). In this article, the dipoles are excited by the BWIT feed network in Fig. 2(b). This feed consists of two microstrip Marchand baluns arranged in parallel to form one differential stripline feed structure. As depicted, the BWIT employs a mirrored series open stub (Z_{oc}) and a parallel short stub (Z_{sc}) in each feed line. As with the Marchand balun, these reactive components mitigate the common mode while scanning. Notably, symmetry between the feed lines is maintained and ensures balanced transmission of opposite phase signals from the feed to the aperture for all scan angles. Finally, a metal via connects the dipole arms on the center layers of the BWIT feed onto the outer layers. Notably, the BWIT structure excites the dipoles through a via shorted to the feed's outer shielding. As with a Marchand balun, the BWIT also relies on the "Γ shaped" feed line to couple to the dipoles through its return path, with the open stub eliminating common modes.

For design, the proposed BWIT feed was simulated as an infinite array without the dipoles in ANSYS HFSS v.19. Fig. 3 shows that the BWIT conveys good amplitude and phase balance with negligible common-mode influence, even when scanning down to 60°. At broadside, the simulated maximum amplitude balance was $\pm$0.01 dB with maximum phase imbalance of $\pm$1.28 degrees. Further, only small phase imbalances are obsereved in the 45° and 60° scanning cases, and these are attributed to the common mode coupling introduced to the feed branches. However, the BWIT still retains a high common-mode rejection ratio (CMRR) $>$27 dB (see [23, Fig. 2]). But this is only an imbalance of $\pm$0.01 dB and maximum phase imbalance $< \pm$1.5°. Further, the average simulated insertion loss was 0.67 dB, 0.86 dB and 1.01 dB over the band for the respective broadside, 45°, and 60° scan cases.

B. DIPOLE ARRAY DESIGN

The dipole array operates at two independent linear polarizations using an egg-crate configuration for ease of assembly (see Fig. 1). Also, a metal frequency selective surface (FSS) superstrate is employed for low-angle scanning with FSS design considerations, following those outlined in [5], [20]. In short, sub-wavelength metallic rectangles are printed above the dipoles as a FSS superstrate. This periodic FSS emulates an effective dielectric constant (ϵ_{eff}) of the impedance matching as a thick dielectric slab above the dipoles. Importantly, that superstrate eliminates the occurrence of trapped waves at deep scan angles (typically $>$ 50°). Capacitive overlap sleeves are included to extend impedance bandwidth by countering the inductance of the ground plane at lower bands [24]. The final design dimensions are given in Fig. 1(c) and Table 1.

C. DIPOLE ARRAY WITH BWIT SIMULATIONS

Infinite array simulations of the array were performed in the balanced mode, using a pair of differential 50Ω lumped ports, excited with 0° and 180° phases [25]. This is denoted in Fig. 2(b). The infinite array active VSWR is given Fig. 4(a). The array provides a broadside VSWR $<$ 3 across 1.05-3.2 GHz, implying an impedance bandwidth ratio of 3:1. Likewise, while scanning down to 45°, the array shows VSWR $<$ 3 across 1.05-3.2 GHz in the E-plane and D-plane and across 1.35-3.2 for the H-plane. Even more, resonant-free VSWR $<$ 3 impedance bandwidth is achieved in the E-plane down to 60°.

As is the case with other perfect electric conductor (PEC) backed dipole arrays, the H-plane scanning VSWR degrades at lower frequencies [5]–[7], [20]. This is primarily due to Floquet mode impedance variations with scanning. Specifically, the $1/cos(\theta)$ term modifies the H-Plane impedance significantly when scanning [26]. Notably, higher order multilayer superstrate matching network improves this mismatch, but at the expense of array profile and complexity [6], [27]. The unit cell H-pol to V-pol port-to-port coupling is also given in Fig. 4(b), showing $>$ 30 dB isolation between the polarizations across all scan angles of interest.

After optimizing the array's infinite array performance, full-wave semi-finite simulations were performed. These results, which include finite edge and ground plane effects,

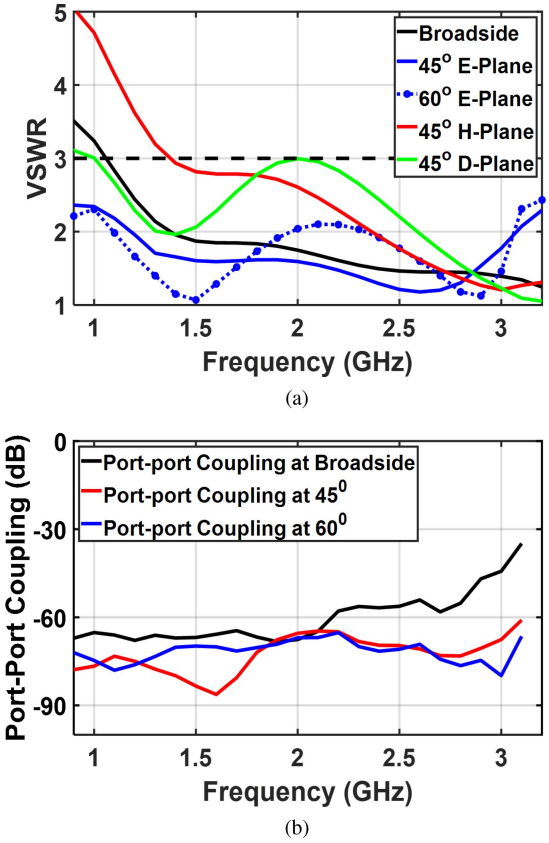

FIGURE 4. (a) Simulated infinite array active VSWR in the E, H, and D-planes of the dipole array at various scan angles, (b) Simulated unit cell H-pol to V-pol (port-to-port) coupling for different scan cases.

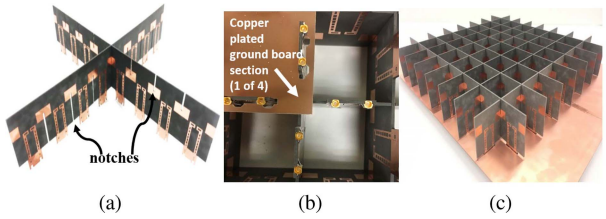

FIGURE 5. (a) Fabricated 8 × 1 antenna strip being assembled as an egg-crate, (b) Feed ports for four antenna elements on the bottom side on the fabricated array, and (c) Fully assembled 8×8 dipole array on 384mm×384mm ground plan.

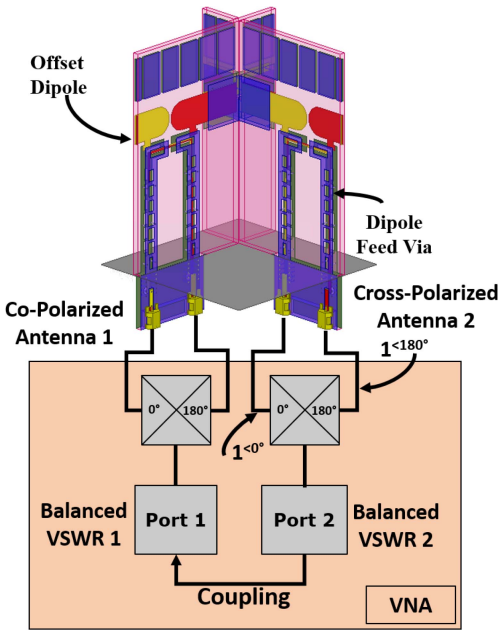

FIGURE 6. Measurement setup employed to characterise balanced S-parameters using the 4-port VNA. *Note:* For gain measurements, an external Marki Bal-0003 balun was used to translate the differential antenna port to the single-ended measurement port.

are presented in the next section along with comparitive measurements.

III. ARRAY FABRICATION AND MEASUREMENTS

A. ARRAY PROTOTYPE FABRICATION

For validation, an 8×8 array prototype, shown in Fig. 5 was fabricated with dimensions as given in Fig. 1(c) and Table 1. The antenna board was constructed from three 0.50 mm (20 mil) Rogers 5880 ($\epsilon_r = 2.2$) laminates, subject to metal tolerance of 0.25 mm (10 mil) and the stackup in Fig. 1. To the best of the authors' knowledge, this is the first differential array that includes both the feed and superstrates on the vertical antenna cards without added fabrication steps, implying a simple implementation. For ease of assembly, notches were cut into the dielectric board outlines to enable an egg-crate arrangement, providing structural stability. No direct electrical connection or soldering was required at the joints. The 384mm×384mm ground board in Fig. 5(a) was milled from four copper-clad 60 mil FR4 board with element cutouts. These four sections were combined with copper tape at the seams to form a lightweight, structurally stable and resonance free ground plane for testing the array. Notably, material choices have consequences beyond electrical properties. For example, the utilized Rogers 5880 material is of exceptional low loss, but is also physically pliable. This can lead to adverse effects in polarization purity, as described below.

Fig. 5(c) shows the feed ports at the bottom side of the ground plane. Notably, the fabricated TCDA houses 256 connectors to excite each antenna element differentially (64-element differential pairs per polarization). Future application-specific beamforming feed network can be designed, determined by the space, weight, and power needs of the application. Coaxial cables would likely be used to feed into a beamforming network. Depending on the availability of existing amplifiers and switches, a printed feed network with integrated balun could also be considered.

B. ARRAY MEASUREMENTS

For measurement, a 4-port Vector Network Analyzer (VNA) was operated in an internally calibrated differential mode. Two ports (ports 1 and 2) of the VNA were employed to create an ideal 180° hybrid coupler to measure the balanced S-parameters for each dipole, as shown in Fig. 6. We computed the active balanced VSWR by adding a linear balanced

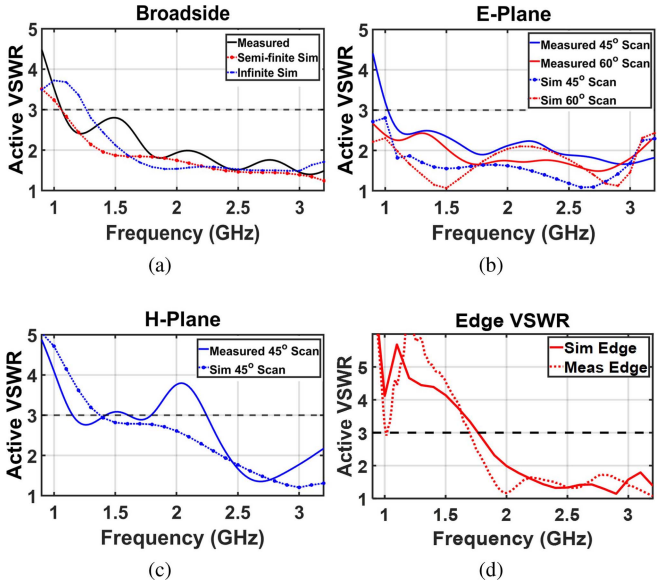

FIGURE 7. Measured active VSWR of an embedded center array element for (a) broadside, (b) E-Plane, (c) H-Plane scanning cases with comparisons to simulation, and (d) edge elements measured active VSWR at broadside.

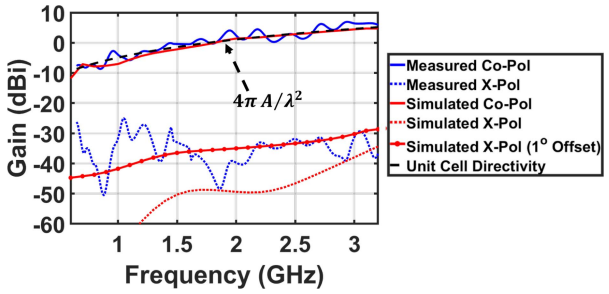

FIGURE 8. Measured vs simulated broadside co-polarized and cross-polarized gain of the center element as a function of frequency. For comparison with measurements, the simulated case of 1° misalignment in ϕ is also given, along with maximum achievable gain.

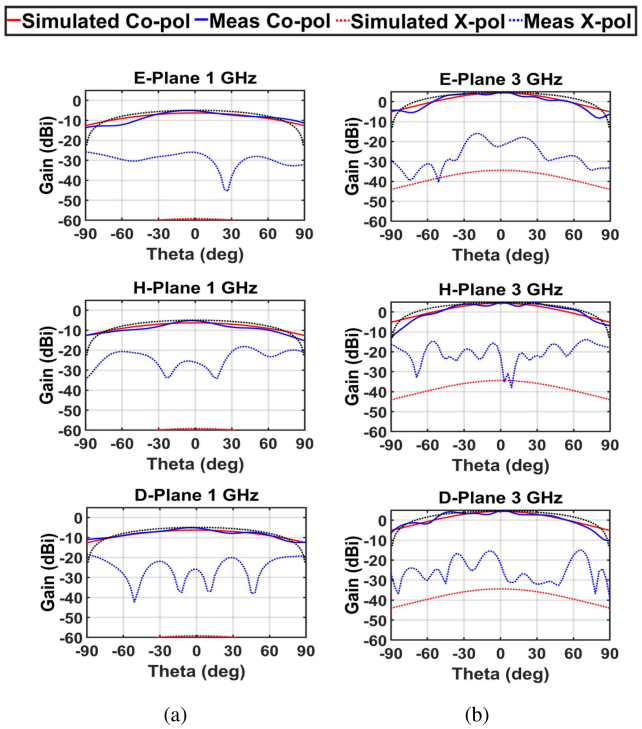

FIGURE 9. Measured embedded patterns of the center element in the E,H and D-planes for (a) 1 GHz, and (b) 3 GHz. Comparisons to simulation are also given. More than 20 dB polarization purity is achieved out to $\theta = \pm 60°$.

reflection coefficient $S_{dd,nn}$ of the embedded center element under test, with a balanced coupling terms $S_{dd,nm}$ [6]. For each measurement, the remaining elements were terminated with 50Ω matched loads.

The measured active VSWR of an embedded center element is depicted in Fig. 7 as a function of frequency with comparison to simulations. As seen, the measured active VSWR yields an 3:1 impedance bandwidth with VSWR < 3 from 1.05 GHz to 3.2 GHz at broadside, in agreement with semi-finite simulations. In fact, a slightly greater impedance bandwidth was measured due to ohmic losses and soldering imperfections. Notably, E-plane and H-plane scanning VSWR closely follows the infinite array simulated values, with VSWR < 3 across the band. There is a mismatch at 2 GHz in the H-plane due to fabrication tolerances and a lack of mutual coupling versus an infinite array. As previously noted, the degraded impedance matching in the H-plane is typical of this array family [6], [20]. In addition, the effect of edge elements on impedance bandwidth is also simulated, as shown in Fig. 7(d). The edge elements have a VSWR < 3 across 1.76 - 3.4 GHz, though in practice these are typically used as matched terminated guard elements.

For gain measurements, an external Marki Bal-0003 balun [28] was used to translate the differential antenna port to the single-ended measurement port. This test component was later de-embedded from the gain measurement. Using this set-up, we measured the embedded center element gain of an otherwise match-loaded 8×8 dual-polarized array, depicted in Fig. 5. The measured broadside co-polarized and cross-polarized gain of an embedded center element is plotted versus frequency in Fig. 8 in comparison to simulations. The array pattern is constructed using the single element measurements with Ludwig's 3^{rd} definition [29]. These are given in Fig. 9. The measured patterns closely follow both the predicted values and the theoretical $4\pi Acos(\theta)/\lambda^2$ gain, where A is the unit-cell area. Due to the measurement equipment being single-ended, the development of a balun–beamforming network would be required to show the radiation patterns of the 8×8 finite dual-polarized array. Instead, the embedded element pattern is shown, as it is well known to be a good indication of the scan performance in a large array [6].

Notably, the differences between the simulated and measured cross-polarized gain levels in Fig. 8 and Fig. 9 stem from the presence of small physical misalignment's. Specifically, even a 1° misalignment can create large disparities in decibel scales [29]. Here, the 1° misalignment refers

TABLE 2. Comparison of UWB dipole arrays.

Reference	Differential	Bandwidth (GHz)	Scan Range (E/H)
[4]	N	8.00-12.5	70 / 60
[5]	N	0.50-3.10	75 / 60
[6]	N	3.53-21.2	60 / 60
[7]	N	0.80-4.38	70 / 55
[8]	N	7.00-18.0	60 / 60
[10]	N	17.0-42.0	45 / 45
[11]	N	2.05-10.3	60 / 45
[12]	N	2.20-3.95	N/A
[9]	Y	0.80-2.50	50 / 50
[13]	Y	1.66-2.80	45 / 45
[18]	Y	3.00-14.0	N/A
[19]	Y	0.30-1.00	45 / 45
This Work	Y	1.05-3.20	60 / 45

to the position of the fabricated V-pol antenna cards relative to the near field chamber's plane of reference used to measure the array. Easily, >30 dB disparities can be introduced [29]. Of course, in simulation the array is perfectly aligned, and so this effect is not present. For comparisons to measurements, the simulated case of 1° misalignment's in ϕ is also given in Fig. 8. As can be seen, 1° misalignment measurement in ϕ can greatly increase the perceived cross-polarized gain values. Even more, extremely small bending of the PCB card could also degrade cross-polarized gain levels. the latter is important when choosing a dielectric substrate.

IV. BENCHMARKING WIDEBAND DIFFERENTIAL DIPOLE ARRAYS

As previously mentioned, the main motivation for a wideband differential array with wide angle scanning is the availability of new differential RF back ends [2]. To show the benefits of the presented array, we provide a comparison to recent works in Table 2. It is seen that the presented array's performance is well aligned with similar differentially-fed arrays (about 3:1 VSWR < 3 impedance bandwidth ratio). Compared to other works that tackle common-modes [18], [19], the lack of attenuating resistors in this work lead to increased efficiency and simple standard PCB fabrication. Also, this boasts the lowest reported angle E-plane scanning, more than the previous 45° or 50° benchmarks [9], [13].

V. CONCLUSION

We presented a dual-polarized dipole array operating from L to S bands (*viz.* 1.05 GHz to 3.2 GHz), specifically targeting 2G to 5G communications bands. The presented novel ultrawideband differential feed, denoted as the Balanced Wideband Impedance Transformer (BWIT), removes common-mode resonances when scanning up to 60° off broadside in the E-plane. In reference to past common-mode mitigation techniques, the BWIT is unparalleled in achieving balanced feeding on low-cost PCB, with no added fabrication steps or losses. Trade-offs between performance, material choice, and antenna profile were discussed. Most importantly, an 8 × 8 differential array was fabricated and measured, with measurements showing agreement to simulations.

REFERENCES

[1] *Radio Spectrum Allocation*. Accessed: Feb. 24, 2020. [Online]. Available: https://www.fcc.gov/engineering-technology/policy-and-rules-division/general/radio-spectrum-allocation

[2] *Zynq UltraScale+ RFSoC*. Accessed: Feb. 24, 2020. [Online]. Available: https://www.xilinx.com/support/documentation/data_sheets/ds889-zynq-usp-rfsoc-overview.pdf

[3] D. M. Pozar, "Microwave engineering education: From field theory to circuit theory," in *IEEE/MTT-S Int. Microwave Symp. Dig.*, 2012, pp. 1–3.

[4] J. A. Kasemodel, C. C. Chen, and J. L. Volakis, "Wideband planar array with integrated feed and matching network for wide-angle scanning," *IEEE Trans. Antennas Propag.*, vol. 61, no. 9, pp. 4528–4537, Sep. 2013.

[5] E. Yetisir, N. Ghalichechian, and J. L. Volakis, "Ultrawideband array with 70° scanning using FSS superstrate," *IEEE Trans. Antennas Propag.*, vol. 64, no. 10, pp. 4256–4265, Oct. 2016.

[6] J. T. Logan, R. W. Kindt, M. Y. Lee, and M. N. Vouvakis, "A new class of planar ultrawideband modular antenna arrays with improved bandwidth," *IEEE Trans. Antennas Propag.*, vol. 66, no. 2, pp. 692–701, Feb. 2018.

[7] A. O. Bah, P. Qin, R. W. Ziolkowski, Y. J. Guo, and T. S. Bird, "A wideband low-profile tightly coupled antenna array with a very high figure of merit," *IEEE Trans. Antennas Propag.*, vol. 67, no. 4, pp. 2332–2343, Apr. 2019.

[8] Z. Zhang, S. Yang, J. Huang, S. Xiao, Y. Chen, and S. Qu, "Wideband tightly coupled dipole arrays with balanced scattering and radiation based on a black-box method," *IEEE Access*, vol. 7, pp. 118402–118410, 2019.

[9] S. Kim and S. Nam, "Bandwidth extension of dual-polarized 1-D TCDA antenna using VMS," *IEEE Trans. Antennas Propag.*, vol. 67, no. 8, pp. 5305–5312, Aug. 2019.

[10] S. M. Moghaddam, J. Yang, and A. U. Zaman, "Fully-planar ultra-wideband tightly-coupled array (FPU-TCA) with integrated feed for wide-scanning millimeter-wave applications," *IEEE Trans. Antennas Propag.*, vol. 68, no. 9, pp. 6591–6601, Sep. 2020.

[11] B. Wang, S. Yang, Y. Chen, S. Qu, and J. Hu, "Low cross-polarization ultrawideband tightly coupled balanced antipodal dipole array," *IEEE Trans. Antennas Propag.*, vol. 68, no. 6, pp. 4479–4488, Jun. 2020.

[12] M. R. Naeini, M. Mirmozafari, and D. van der Weide, "Monolithic 3-D printing of an integrated marchand balun with a dipole antenna," *IEEE Trans. Compon. Packag. Manuf. Technol.*, vol. 10, no. 4, pp. 654–658, Apr. 2020.

[13] Z. Tang, J. Liu, R. Lian, Y. Li, and Y. Yin, "Wideband differentially fed dual-polarized planar antenna and its array with high common-mode suppression," *IEEE Trans. Antennas Propag.*, vol. 67, no. 1, pp. 131–139, Jan. 2019.

[14] D. Cavallo, A. Neto, and G. Gerini, "PCB slot based transformers to avoid common-mode resonances in connected arrays of dipoles," *IEEE Trans. Antennas Propag.*, vol. 58, no. 8, pp. 2767–2771, Aug. 2010.

[15] S. G. Hay and J. D. O'Sullivan, "Analysis of common-mode effects in a dual-polarized planar connected-array antenna," *Radio Sci.*, vol. 43, no. 6, pp. 1–9, Dec. 2008.

[16] J.-P. R. Bayard, D. H. Schaubert, and M. E. Cooley, "E-plane scan performance of infinite arrays of dipoles printed on protruding dielectric substrates: Coplanar feed line and E-plane metallic wall effects," *IEEE Trans. Antennas Propag.*, vol. 41, no. 6, pp. 837–841, Jun. 1993.

[17] S. Edelberg and A. Oliner, "Mutual coupling effects in large antenna arrays II: Compensation effects," *IRE Trans. Antennas Propag.*, vol. 8, no. 4, pp. 360–367, Jul. 1960.

[18] J. J. Lee, S. Livingston, and R. Koenig, "Performance of a wideband (3-14 GHz) dual-pol array," in *Proc. IEEE Antennas Propag. Soc. Symp.*, vol. 1, 2004, pp. 551–554.

[19] E. de Lera Acedo, E. Garcia, V. Gonzalez-Posadas, J. L. Vazquez-Roy, R. Maaskant, and D. Segovia, "Study and design of a differentially-fed tapered slot antenna array," *IEEE Trans. Antennas Propag.*, vol. 58, no. 1, pp. 68–78, Jan. 2010.

[20] J. Zhong, A. Johnson, E. A. Alwan, and J. L. Volakis, "Dual-linear polarized phased array with 9:1 Bandwidth and 60° scanning off broadside," *IEEE Trans. Antennas Propag.*, vol. 67, no. 3, pp. 1996–2001, Mar. 2019.
[21] M. H. Novak, F. A. Miranda, and J. L. Volakis, "Ultra-wideband phased array for millimeter-wave ISM and 5G bands, realized in PCB," *IEEE Trans. Antennas Propag.*, vol. 66, no. 12, pp. 6930–6938, Dec. 2018.
[22] W. Elsallal, J. Hood, A. Locker, and R. Kindt, "Frequency-scaled ultra-wide spectrum element," U.S. Patent 9 991 605 B2, 2019.
[23] D. Jorgesen and C. Marki, *Balun Basics Primer*. Morgan Hill, CA, USA: Marki Microw., 2015, pp. 1–3.
[24] E. A. Alwan, K. Sertel, and J. L. Volakis, "Circuit model based optimization of ultra-wideband arrays," in *Proc. IEEE Int. Symp. Antennas Propag.*, 2012, pp. 1–2.
[25] D. E. Bockelman and W. R. Eisenstadt, "Combined differential and common-mode scattering parameters: Theory and simulation," *IEEE Trans. Microw. Theory Techn.*, vol. 43, no. 7, pp. 1530–1539, Jul. 1995.
[26] H. Wheeler, "Simple relations derived from a phased array made of an infinite current sheet," in *Proc. Antennas Propag. Soc. Int. Symp.*, vol. 2, 1964, pp. 157–160.
[27] D. Cavallo, W. H. Syed, and A. Neto, "Connected-slot array with artificial dielectrics: A 6 to 15 GHz dual-pol wide-scan prototype," *IEEE Trans. Antennas Propag.*, vol. 66, no. 6, pp. 3201–3206, Jun. 2018.
[28] *Bal003*. Accessed: Feb. 24, 2020. [Online]. Available: https://www.markimicrowave.com/Assets/datasheets/BAL-0003.pdf?v=072320
[29] A. Ludwig, "The definition of cross polarization," *IEEE Trans. Antennas Propag.*, vol. 21, no. 1, pp. 116–119, Jan. 1973.